

Sensitivity Analysis and Optimization of Geometric Parameters of a New Fluid Bag Buffer Mechanism on Buffering Performance

WANG Hongxian^{1,2}, HOU Yu³, ZHANG Ming², NIE Hong^{4*}

1. Key Laboratory of Advanced Technology of Small and Medium-Sized UAV Ministry of Industry and Information Technology, Nanjing University of Aeronautics and Astronautics, Nanjing 210016, P. R. China;

2. State Key Laboratory of Mechanics and Control of Mechanical Structures, Nanjing University of Aeronautics and Astronautics, Nanjing 210016, P. R. China;

3. School of Aeronautic Engineering, Nanjing Vocational University of Industry Technology, Nanjing 210023, P. R. China;

4. Key Laboratory of Fundamental Science for National Defense-Advanced Design Technology of Flight Vehicle, Nanjing University of Aeronautics and Astronautics, Nanjing 210016, P. R. China

(Received 8 December 2021; revised 2 March 2022; accepted 28 April 2022)

Abstract: A new fluid bag buffer mechanism, which can provide large axial stiffness under the small displacement, is designed. The dynamic change laws of the mechanism stiffness and the internal pressure of the fluid bag are studied when it is subjected to impact load. According to the protection performance for the flexible joint and the pressure change in the fluid bag during the impact process, the sensitivity of the geometric parameters of the fluid bag to the axial stiffness is analyzed by using the orthogonal experimental method, and the optimal parameter combination of the geometric parameters of the fluid bag under impact is obtained, leading to the displacement of the inner shell reduce by 41.4%. The results show that the internal pressure of the fluid bag is a rising process of oscillation and fluctuation. The sensitivity of the geometric parameters of the fluid bag to the displacement of the inner shell from high to low is as follows: Height H , radius r , wall thickness t , chamfer A . The correlation between the geometric parameters of the fluid bag and its internal pressure is: H is negatively correlated with the internal pressure, while the r , t , and A are positively correlated with the internal pressure.

Key words: fluid bag buffer mechanism; flexible joint; axial stiffness characteristics; orthogonal experiment method; internal pressure of fluid bag

CLC number: TH135

Document code: A

Article ID:1005-1120(2022)05-0569-15

0 Introduction

With the continuous improvement of safety and reliability requirements of mechanical mechanism, different types of buffers are designed to prevent rigid collision due to impact load, reduce vibration and noise, and improve the quality and life of mechanism. In this paper, a buffer which can withstand large impact load in a small displacement is studied. The fluid bag in the new buffer mechanism adopts nearly incompressible liquid, which can absorb a

large amount of energy in small deformation and recover quickly. The flexible composite material is used in the contact part between the buffer fluid bag and the mechanism, which can fit the mechanism well under the impact load, so as to prevent the damage of the mechanism caused by stress concentration.

At present, there are few research on fluid bags with liquid as medium at home and abroad. However, the research on buffer airbags and air

*Corresponding author, E-mail address: hnie@nuaa.edu.cn.

How to cite this article: WANG Hongxian, HOU Yu, ZHANG Ming, et al. Sensitivity analysis and optimization of geometric parameters of a new fluid bag buffer mechanism on buffering performance[J]. Transactions of Nanjing University of Aeronautics and Astronautics, 2022, 39(5):569-583.

<http://dx.doi.org/10.16356/j.1005-1120.2022.05.006>

springs similar to buffer fluid bag is still deep. Similar to the working principle of the fluid bag buffer, the buffer airbag and air spring charge gas into the flexible shell. Tutt et al.^[1] introduced the test of a kind of space exploration vehicle's falling impact on the ground, in which the buffer airbag was used for protection. Erin et al.^[2] proposed a new modeling method for rubber airbags, which used linear spring, damper and hysteresis damper in parallel, and could approximately model the rubber airbag. Berg^[3-4] adopted a new approximation method. When modeling the rubber airbag part of the air spring, the nonlinear characteristic model of the rubber airbag composed of linear elastic model, friction model and Maxwell model was used for modeling and analysis. Based on the theory of the elastic support damping, Oda et al.^[5] established the Nishimura model. The new simulation model had a wider application range and could be used for simulation analysis of air springs in wide frequency domain. Yuasa et al.^[6] carried out simulation modeling and analysis on rubber airbags, studied its structure and mechanical characteristics, and optimized the design of air springs. Lee et al.^[7-8] also simulated the diaphragm air spring, studied various mechanical properties of the rubber airbag, analyzed the influence of various factors on its mechanical characteristics, and studied the influence of initial filling pressure, cord and other factors on the deformation of the air bag, as well as the mechanical characteristics of the air spring. Jeong et al.^[9] used rebar, shell and Halpin tsal elements to conduct finite element modeling of air springs, and studied the change of mechanical properties of rubber airbags under the influence of different cord angles, and carried out experimental verification. Wong et al.^[10] studied the mechanical characteristics of a new air spring, and studied the effects of various factors on its dynamic and static stiffness. Oman et al.^[11] introduced the influence of piston geometric parameters of air springs on its load deflection characteristics and fatigue life, considered two kinds of piston shapes, compared their load deflection characteristics and fatigue life, predicted the fatigue life and the final failure time and global position of air springs, and compared the actual mea-

sured results with the predicted results. Li et al.^[12] proposed an improved finite element method, which could be used to solve the problem that the mechanical behavior of the air spring was controlled by the multi-directional thermodynamic process of the closed air. The results showed that the method was reliable and effective. Zhu et al.^[13] established a generalized analysis model to predict the amplitude and frequency dependent characteristics of the air spring, and established an accurate finite element simulation model of the air spring considering the thermodynamics of the pneumatic system of the bellows tank, the effective friction and viscoelastic damping of the bellows rubber. Heinrich et al.^[14] compared the effects of two different cord setting methods on the local rubber matrix strain and stress of air springs, adopted a method that considered both the geometric shape of cord and the filament structure of cord, and analyzed the global model and sub model of cyclic symmetrical cross section including bellows. Li et al.^[15] proposed and developed a hybrid vibration isolator composed of Maglev actuators and air springs. The performance of the hybrid isolator is experimented. The flexible gap protection technology and detachable mounting structure are used to improve the stability and adaptability of the hybrid vibration isolator in the marine environment.

To sum up, the research on air springs and buffer airbags at home and abroad mostly focuses on the influence of various materials and geometric parameters of rubber airbags on the mechanism stiffness^[16]. It is instructive to study the influence of geometric parameters of the buffer fluid bag on its mechanical properties^[17]. In this paper, taking a certain type of fluid bag buffer mechanism as the research object, the axial stiffness and internal pressure of the fluid bag in the working process are studied. Through the analysis and optimization of the buffer mechanism, the buffer performance of the buffer mechanism is improved and the safety of the fluid bag is enhanced. According to the change of axial stiffness and internal pressure of fluid bags during the impact process, the sensitivity of each geometric parameter of fluid bags to the change of axial stiffness is analyzed by the orthogonal experimental

method, and the optimal parameter combination of each geometric parameter of fluid bags under impact is obtained. The safety performance and buffering performance of the fluid bag under the actual working state are improved, which lays a foundation for the research of this new type of buffers.

1 Working Process Analysis of Fluid Bag

1.1 Introduction of buffer mechanism of fluid bag

The buffer mechanism is mainly composed of two parts, one is the flexible joint, the other is the fluid bag. The mechanism is shown in Fig.1(a). When the mechanism works, a large axial upward impact load is adopted at the bottom of the mechanism.

The flexible joint consists of a rubber layer and a metal layer, in which the metal plate and the rubber layer are bonded together. The material properties of the flexible joint are as shown in Table 1. They should not have large axial static displacement; otherwise the flexible joint may fail and cause the mechanism failure. Therefore, it is necessary to

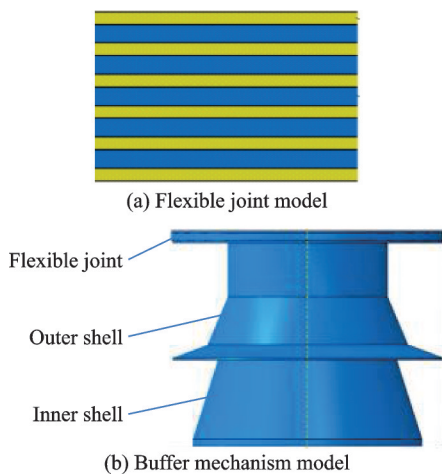


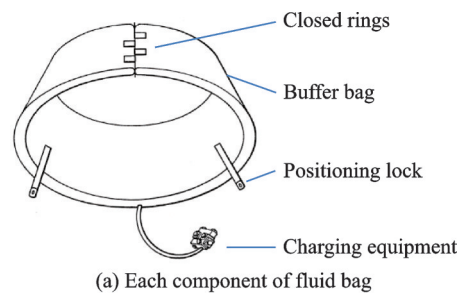
Fig.1 Fluid bag buffer mechanism

Table 1 Material properties of flexible joint

Layer type	C10	C01	C20	Elastic modulus/MPa	Poisson's ratio
Metal layer				12 000	0.1
Rubber layer	0.061	0.429	0.023		0.495

use large stiffness buffer mechanism for axial protection of the flexible joint. It is assumed that there is absolute adhesion between the elastic layer and the metal layer. The flexible joint is shown in Fig.1(b).

As shown in Fig.2(a), the fluid bag is a kind of conical ring flexible sealing container filled with approximately incompressible fluid. The real fluid bag is not connected in the ring direction, and the head end and tail end of the fluid bag have a closed ring, which is inserted with a hinge pin to lock the fluid bag in the mechanism^[18-19]. The charging pipe is connected with the joint and the bottom of the fluid bag to realize the charging of the fluid bag. The connector is connected to the liquid filling device at the same time. The pressure of the fluid bag can be adjusted to a predetermined value, and the fluid bag can be placed between the inner shell and the outer shell, which can greatly reduce the load transmitted to the flexible joint through the contact area between the inner shell and the outer shell. The simplified fluid bag model is shown in Fig.2(b).



(a) Each component of fluid bag



(b) Simplified model of fluid bag

Fig.2 Fluid bag

1.2 Numerical method analysis of fluid bag

When the liquid reaches the static equilibrium state in the fluid bag, there is no tension and tangential force between the liquid particles or between the liquid and the fluid bag, but there is only normal pressure, which is the hydrostatic pressure. In the

fluid bag, the hydrostatic pressure has two important characteristics: Firstly, in the fluid bag, the action direction of the liquid pressure is vertical and points to the wall of the fluid bag. Secondly, when the liquid is still in the fluid bag, the hydrostatic pressure of any liquid particle is the same in all directions.

The hydrostatic pressure acting on any point of the liquid in the fluid bag is the same in every direction, which is independent of the normal direction of the pressure action surface, that is, independent of the shape of the fluid bag. Since the liquid in the fluid bag is a continuous medium, its hydrostatic pressure is a continuous function related to the spatial coordinates. Therefore, it can be concluded that

$$p = f(x, y, z) \quad (1)$$

A small parallelepiped is randomly selected from the liquid in the fluid bag. The sides of the six faces are dx , dy , and dz , respectively, and they are parallel to the three coordinate axes. Let the projection of the unit mass force on the coordinate axis be f_x , f_y , and f_z . The components of the mass force in x , y , and z axes are $\rho f_x dx dy dz$, $\rho f_y dx dy dz$, and $\rho f_z dx dy dz$, respectively, where the surface force is the hydrostatic pressure. Let the hydrostatic pressure at any point in the hexahedron be p , then the hydrostatic pressure at the center of the two surfaces parallel to the x axis in the normal direction is divided into

$$p - \frac{dx}{2} \frac{\partial p}{\partial x}, p + \frac{dx}{2} \frac{\partial p}{\partial x} \quad (2)$$

Because the hexahedron is a small hexahedron, the average hydrostatic pressure in the plane can be regarded as equal to the pressure at the central point. Therefore, the hydrostatic pressure of the fluid on these two surfaces is

$$\left(p - \frac{dx}{2} \frac{\partial p}{\partial x} \right) dy dz, \left(p + \frac{dx}{2} \frac{\partial p}{\partial x} \right) dy dz \quad (3)$$

Since the sum of all the external force vectors acting on the hexahedron is 0, for the x axis, it can be obtained that

$$\rho f_x dx dy dz + \left(p - \frac{dx}{2} \frac{\partial p}{\partial x} \right) dy dz - \left(p + \frac{dx}{2} \frac{\partial p}{\partial x} \right) dy dz = 0 \quad (4)$$

After simplification, it can get the following results

$$f_x - \frac{\partial p}{\rho \partial x} = 0 \quad (5)$$

Similarly, the results can be obtained on the y and z axes. Then, when the liquid in the fluid bag is in equilibrium, the differential equations are as follows

$$\begin{cases} f_x - \frac{\partial p}{\rho \partial x} = 0 \\ f_y - \frac{\partial p}{\rho \partial y} = 0 \\ f_z - \frac{\partial p}{\rho \partial z} = 0 \end{cases} \quad (6)$$

According to the equation, when the liquid in the fluid bag is at rest, the change rate of the hydrostatic pressure along any axis is equal to its unit mass force.

In the fluid bag, compared with the external force, the pressure change caused by the liquid mass force is negligible. Therefore, in Eq.(6), f_x , f_y , and f_z can be regarded as 0. Therefore, the following results are obtained

$$\frac{\partial p}{\partial x} = 0, \frac{\partial p}{\partial y} = 0, \frac{\partial p}{\partial z} = 0 \quad (7)$$

That is, the change rate of the hydrostatic pressure of the liquid in the fluid bag along any axis is 0. Combined with the second characteristic of the hydrostatic pressure, it can be known that the pressure in the fluid bag is equal everywhere.

Finally, the finite element method is used to divide the fluid bag shell and liquid into fine meshes. Because the liquid pressure is equal everywhere, the pressure of each liquid unit is also the same, and the volume (density) of the liquid is related to temperature and pressure. Therefore, this paper will mesh a set of all liquid units, and set a reference point for this set, and assign the initial pressure and density of all liquid units on the reference point, so as to complete the real simulation of the fluid bag.

1.3 Establishment of finite element analysis model of fluid bag buffer mechanism

According to the structural characteristics of the fluid bag buffer mechanism, the mechanical anal-

ysis model of the fluid bag buffer mechanism is established using ABAQUS. S4R mesh is used to define the fluid bag, the inner shell and the outer shell. C3D8 mesh is used to define the flexible joint. It is assumed that the mass and temperature of the fluid in the bag remain unchanged during the process. The fluid chamber method is used to couple the liquid chamber and the fluid bag through the reference point. The fluid cavity method in ABAQUS can be used to calculate the liquid-structure interaction based on the surface defined fluid strength. When defining the fluid cavity, the properties of the filling in the fluid cavity can be defined by the reference point (RP), where the RP has coupling with the fluid cavity. The real contact between the fluid bag and the inner shell and the outer shell is established with this method. Finally, the finite element model of the fluid bag buffer mechanism is completed, as shown in Fig.3.

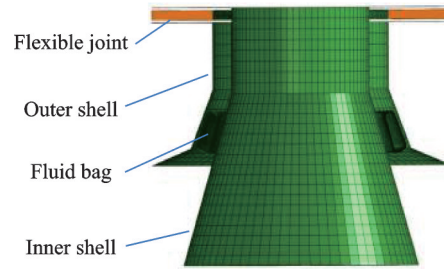


Fig.3 Finite element model of mechanism

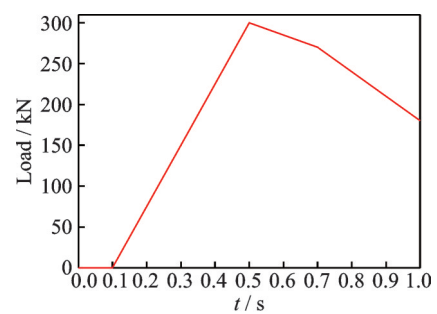
The filling material inside the fluid bag is water. The reason is that after the buffer task is completed, the water in the fluid bag can be discharged to reduce the weight of the buffer mechanism. Set the properties of the water, the temperature is $20\text{ }^{\circ}\text{C}$, and the density is $1.0\text{e}-06\text{ kg/mm}^3$. The material of the buffer mechanism is high strength steel. The fluid bag is made of composite materials. The relevant material properties are shown in Table 2.

Table 2 Material properties of model

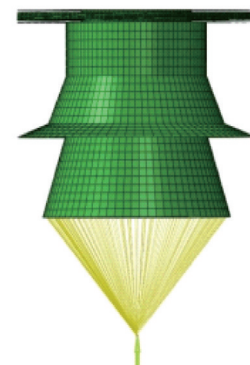
Material	Density/ ($\text{kg}\cdot\text{mm}^{-3}$)	Elastic modulus/ MPa	Poisson's ratio	Bulk modulus/ MPa	Rayleigh damping α	Rayleigh damping β
High strength steel	$7.8\text{e}-06$	$2.1\text{e}+05$	0.3	N/A	3	0
Compound material	$1.4\text{e}-06$	$7.0\text{e}+03$	0.3	N/A	2.96	$1.2\text{e}-04$
Water	$1.0\text{e}-06$	N/A	N/A	$2.18\text{e}+03$	N/A	N/A

In the actual working process of the fluid bag buffer mechanism, it will be subjected to strong impact load. Typical external input curve is shown in Fig.4(a). The load is applied to the bottom of the mechanism in a short time, and then gradually decreases. Therefore, the concentrated load is set to act on the bottom of the inner shell, and the load acts on the load coupling reference node in the model, so that the load is distributed on the bottom surface of the inner shell, as shown in Fig.4(b). The initial pressure of the fluid bag is 2.5 MPa, and the impact load on the bottom of the inner shell is 300 kN. Before the impact load, the fluid bag is pressurized to 2.5 MPa. Then, the inner shell is released and the impact load is used. The impact load increases from 0 N to 300 kN in 0.1—0.5 s, and then decreases gradually.

Mesh independence test is an important task of



(a) External impact load curve



(b) Impact load condition

Fig.4 Impact load case

finite element analysis (FEA). The mesh independence test is analyzed. Considering the accuracy and time, 10 mm mesh size is chosen, as shown in Table 3.

Table 3 Mesh independence test

Test content	Mesh size/mm			
	2.5	5	10	20
Maximum stress of fluid bag/MPa	32.7	32.8	32.6	27.8
Time of fluid bag/s	643	401	307	206

1.4 Simulation result analysis and experimental verification

After the simulation model of the fluid bag buffer mechanism is established, the mechanical characteristics of the fluid bag buffer mechanism are analyzed. The stress map of the fluid bag can be obtained, as shown in Fig.5. It can be seen from the figure that under the action of load, the inner shell moves upward along the axis, the fluid bag deforms with the axial displacement of the inner shell, and the stress map is evenly distributed in the circumferential direction. On the surface of the fluid bag, the stress is concentrated in the lower part of the inner side of the fluid bag and the upper part of the outer side of the fluid bag. The maximum stress is located in the top part of the outside of the fluid bag.

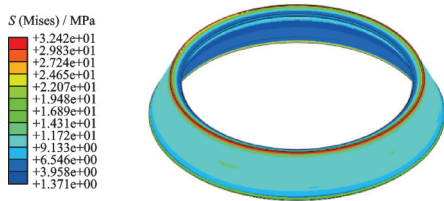


Fig.5 Stress map of fluid bag when maximum load

The dynamic stress map within 0—1.1 s after the impact load is applied is shown in Fig.6. The results show that during the dynamic deformation process, the stress map is evenly distributed in the circumferential direction, and the stress is larger in the lower and upper parts of the fluid bag. During the loading process of impact load, the stress of the fluid bag increases gradually and reaches the peak value about 0.5 s, and then the stress on the fluid bag decreases.

Fig.7 is the stress curve of the element with the

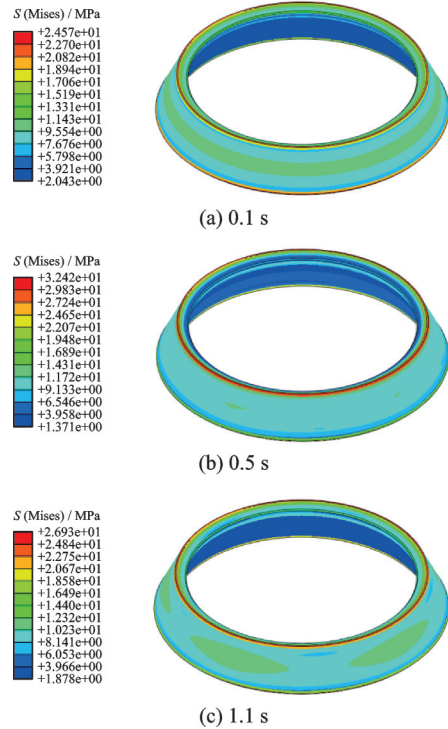


Fig.6 Stress map of fluid bag dynamic process

maximum stress value in the fluid bag from 0 s to 1.1 s. The results show that in the initial stage of 0—0.1 s, the process is the filling stage of the fluid bag. When the pressure of the fluid bag increases from 0 MPa to 2.5 MPa, the element stress will rapidly increase to a fixed value; in the stage of 0.1—0.3 s, due to the existence of initial pressure of 2.5 MPa, the stress is in dynamic oscillation state at this stage with the increase of load, and the stress does not increase significantly; at the stage of 0.3—0.5 s, the stress of the element increases with the increase of load, at 0.5 s, the stress and load reach the maximum value at the same time; at the stage of 0.5—1.1 s, the load begins to decrease, and the stress of the element also begins to decrease; at

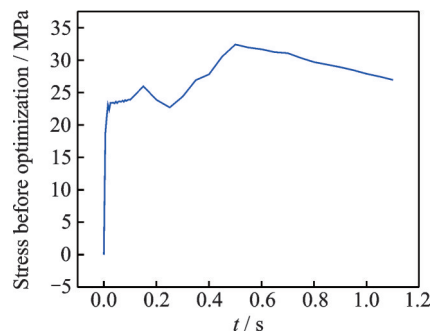


Fig.7 Stress curve of maximum stress element

1.1 s, the load becomes half of the maximum value, and the stress value of the element returns to the same value as that of the oscillation stage.

Fig.8 is the axial displacement map of the fluid bag. It can be seen that under the action of load, the inner shell moves upward along the axial direction, and the fluid bag deforms with the axial displacement of the inner shell, and the displacement map is evenly distributed in the circumferential direction. On the surface of the fluid bag, the position of the maximum absolute displacement is located in the blue part outside the fluid bag. The displacement at this position is due to the existence of the fluid bag initial filling pressure of 2.5 MPa. When the fluid bag is squeezed, the downward displacement occurs; at the same time, the positive axial displacement of the red part on the inner surface of the fluid bag is the largest, which is caused by the upward impact of the load. The minimum displacement is located at the green position of the top and bottom of the fluid bag, and the displacement at this position is almost zero, that is, there is no change in the displacement. It shows that the fluid bag has a strong resistance to deformation.

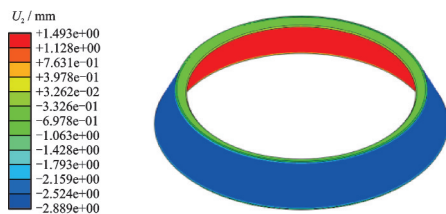


Fig.8 Axial displacement map of fluid bag with maximum load

As shown in Fig.9, it is the displacement curve of the inner shell from 0 s to 1.1 s, which represents the axial stiffness performance of the liquid bag. The results show that in the initial stage of 0—0.1 s, the pressure of the fluid bag increases from 0 MPa to 2.5 MPa, and the displacement of the inner shell oscillates around 0.5 mm; at the stage of 0.1—0.5 s, the load begins to be loaded. With the increase of load, the displacement of the inner shell gradually increases and reaches its maximum position; in the stage of 0.5—1.1 s, it can be seen from Fig.4 that with the decrease of load, the displace-

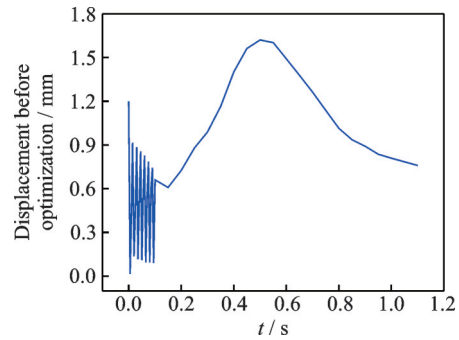


Fig.9 Displacement curve of inner shell

ment of the inner shell begins to decrease and returns to the initial position. It can be seen that it has a great axial stiffness characteristic, the inner shell axial only changing about 1.6 mm, indicating that it has excellent buffering characteristics against large impact force.

Fig.10 is the experimental and simulation curves of the internal pressure of the fluid bag under the dynamic impact load. The experimental data are obtained from the experiment completed in the laboratory by Zhang et al.^[20] Compared with the experimental data and simulation data, it can be seen that the initial filling pressure of the fluid bag is 2.5 MPa. At 0.1 s, the internal pressure of the fluid bag tends to oscillate and increase gradually, and the oscillation amplitude gradually decreases. At 0.5 s, the load reaches the maximum value, and the internal pressure of the fluid bag reaches the maximum value, and then gradually decreases. It can be seen that the overall trend of the simulation result is close to the experimental result, and the agreement is good in the initial step-up stage. It proves the accuracy of the model.

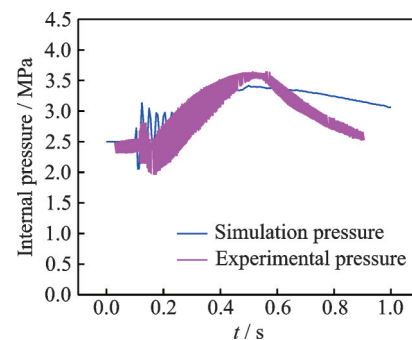


Fig.10 Internal pressure curves of fluid bag during dynamic loading

2 Optimization of Geometric Parameters for Axial Stiffness of Fluid Bag Buffer Mechanism

The displacement of the inner shell represents the axial stiffness of the new fluid bag buffer mechanism. Greater the axial stiffness, better the protection of the flexible joint. It can be seen from the analysis results in Section 1.4 that the inner shell is displaced after loading, and the internal pressure of the fluid bag increases correspondingly. In order to study the variation law of the inner shell displacement and the internal pressure of the fluid bag, the influence and sensitivity of the geometric parameters of the fluid bag on the displacement of the inner shell are analyzed by orthogonal experiments.

2.1 Orthogonal experiment design

Orthogonal experiment method is an experimental design method that uses orthogonal table to select representative combinations from all experimental combinations, and process and analyze these experimental data to obtain the most appropriate combination.

In this paper, the influence of geometry parameters of the fluid bag on the displacement of the inner shell is studied. Through the analysis of the fluid bag structure and the previous engineering practice experience, we know that there are four main geometric design parameters of the fluid bag, which are the height H , the radius r , the chamfer A and the shell thickness t of the fluid bag, as shown in Fig.11 and Table 4.

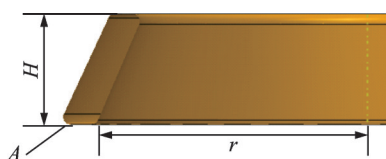


Fig.11 Geometric parameters of fluid bag

Table 4 Initial geometric parameters of fluid bag

Parameter	H/mm	r/mm	A/mm	t/mm
Value	150	300	10	10

Taking H , r , A and t as experimental factors, an orthogonal experimental design with 4 factors and 5 levels can be obtained, as shown in Table 5.

Table 5 Orthogonal experimental design of fluid bag

Level	Parameter/mm			
	H	r	A	t
1	100	260	4	4
2	125	280	7	7
3	150	300	10	10
4	175	320	13	13
5	200	340	16	16

2.2 Orthogonal experiment result

According to the experimental scheme shown in Table 5, the total number of experiments with 4 factors and 5 levels is 54 groups, which is very large and cannot be tested one by one in production practice and scientific research. However, with the method of orthogonal experimental method, only 25 groups of experiments are needed to obtain the optimal combination scheme. Secondary development of ABAQUS, which uses Python, is used to quickly modify the relevant parameters of the model. The results of mechanical analysis of the model are shown in Table 6.

According to the analysis results in Table 6, the mean, range and variance of experimental results corresponding to each level of geometric parameters of the fluid bag are calculated, and then the orthogonal experimental analysis table can be obtained, as shown in Table 7.

T_1 , T_2 , T_3 , T_4 and T_5 in the table represent the average displacement of the inner shell under each level of each factor. The influence of the horizontal variation of each factor on the axial stiffness is reflected by the range r under each level of the same factor. The significant difference of the axial stiffness caused by the level change of each factor is evaluated by the variance S under each level of the same factor. The larger the range r and variance S are, the greater the influence of the horizontal variation of the geometric parameter on the axial stiffness, the more significant and the higher the sensitivity.

Table 6 Orthogonal experiment results of fluid bag

Experiment serial number	Variable parameter				Calculation result
	H/mm	r/mm	A/mm	t/mm	Displacement of inner shell /mm
1	100	260	4	4	6.024
2	100	280	7	7	4.788
3	100	300	10	10	4.107
4	100	320	13	13	4.75
5	100	340	16	16	4.406
6	125	260	7	10	1.696
7	125	280	10	13	1.808
8	125	300	13	16	2.183
9	125	320	16	4	1.986
10	125	340	4	7	1.347
11	150	260	10	16	1.331
12	150	280	13	4	1.108
13	150	300	16	7	1.818
14	150	320	4	10	1.724
15	150	340	7	13	0.855
16	175	260	13	7	4.646
17	175	280	16	10	3.990
18	175	300	4	13	3.561
19	175	320	7	16	2.798
20	175	340	10	4	2.456
21	200	260	16	13	5.906
22	200	280	4	16	5.235
23	200	300	7	4	6.228
24	200	320	10	7	5.537
25	200	340	13	10	3.500

Table 7 Orthogonal experiment analysis of fluid bag

Average displacement of each level	H/mm	r/mm	A/mm	t/mm
T ₁	4.815	3.921	3.578	3.560
T ₂	1.804	3.386	3.273	3.627
T ₃	1.367	3.579	3.049	3.003
T ₄	3.490	3.359	3.237	3.376
T ₅	5.281	2.512	3.621	3.191
R	3.914	1.408	0.573	0.624
S	3.054	0.270	0.059	0.067

According to Table 7, the results of range analysis and variance analysis are consistent. The sensitivity of the geometric parameters of the fluid bag to the displacement of the inner shell from high to low is: H , r , t , and A . The influence curves of geometric parameters of fluid bag are as shown in Fig.12.

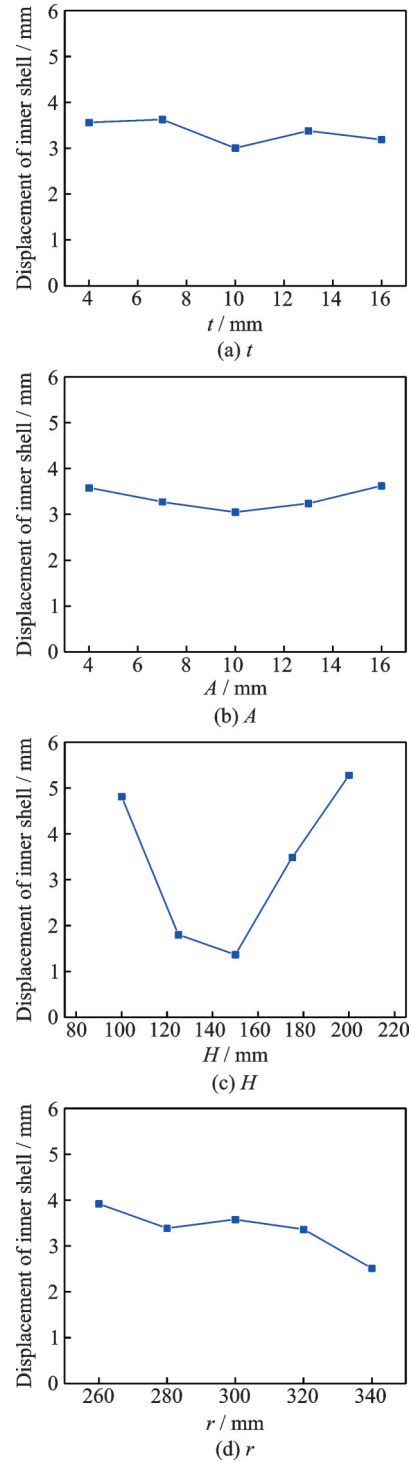


Fig.12 Influence curves of geometric parameters of fluid bag

To sum up, the optimal scheme can be obtained, as shown in Table 8.

Table 8 Geometric parameters after optimization of fluid bag

Factor	H/mm	r/mm	A/mm	t/mm
Value	150	340	10	10

2.3 Analysis of optimized results

According to the above optimal parameters, the optimization model of the fluid bag buffer mechanism is established. The same method is used to simulate the fluid bag, and the stress map of the optimized fluid bag is obtained, as shown in Figs.13—14. By comparing with the stress map before optimization, it can be known that their common characteristics are: The axial distribution is uniform, and the stress changes smoothly in the dynamic process. The difference between them is that the stress concentration area at the top disappears, the maximum stress position is located at the external chamfer of the bottom, and the stress of the whole bottom increases.

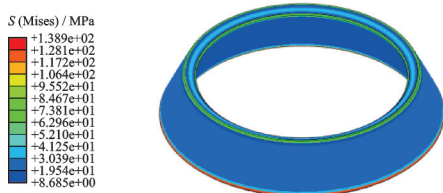


Fig.13 Stress map of fluid bag at maximum load after optimization

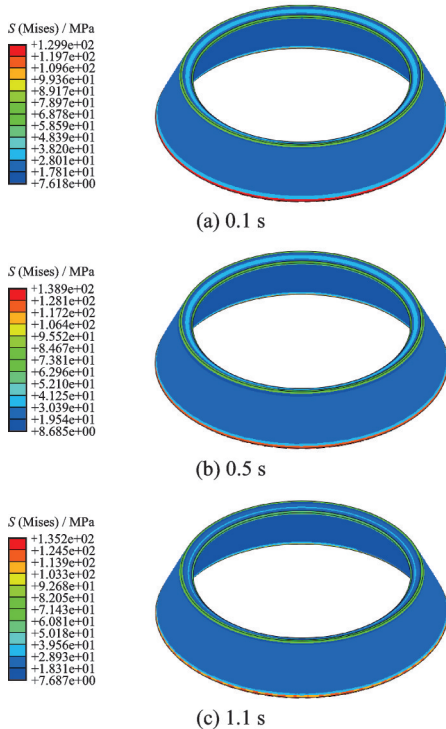


Fig.14 Stress map of dynamic process of optimized fluid bag

The optimized displacement map is shown in Fig.15. Compared with the displacement map before optimization, it can be known that their common characteristics is that the axial displacement distribution in the whole deformation process is uniform; their difference is that the axial displacement of the fluid bag is all vertical downward, and the position of the maximum displacement is at the bottom of the fluid bag.

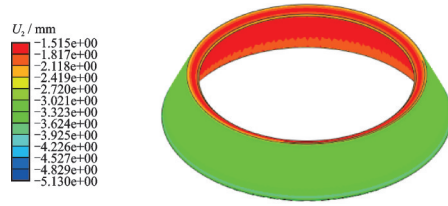


Fig.15 Axial displacement map of fluid bag at maximum load after optimization

Fig.16 is the inter shell displacement and internal pressure curves of the fluid bag before and after optimization under the dynamic impact load. Comparing the curves before and after optimization, it can be known that their common characteristics is: The internal pressure of the fluid bag shows an increasing trend of oscillation, and the amplitude of

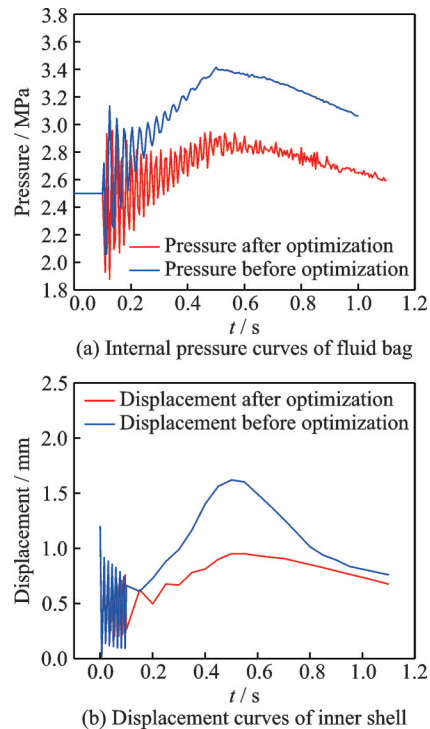


Fig.16 Comparison of buffer performance curves before and after optimization

oscillation decreases with the increase of load. The displacement curve of the inner shell oscillates at a fixed value when the initial pressure is used. After the inter shell is subjected to impact load, the displacement curve begins to increase. At 0.5 s, the load value reaches the maximum value, and then the internal pressure of the fluid bag and the displacement of the inner shell reaches the maximum value, and then gradually decreases. Their differences are as follows: The maximum pressure in the fluid bag is reduced from 3.4 MPa to 3.0 MPa, and the pressure is reduced by 13.3%; the maximum displacement of the inner shell is reduced from 1.62 mm to 0.95 mm, and the displacement is reduced by 41.4%.

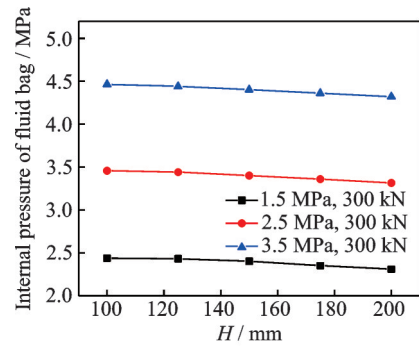
3 Influence of Geometric Parameters of Fluid Bag on Its Internal Pressure

The sensitivity of r , t , A and H to the axial stiffness of the buffer mechanism is obtained by analysis. At the same time, the geometric parameters also affect the internal pressure of the bag. Therefore, the internal pressure changes of the fluid bag under different working conditions are analyzed.

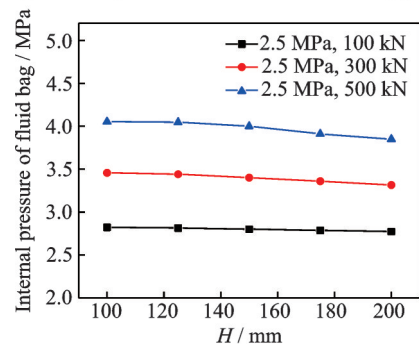
3.1 Influence of height on internal pressure of fluid bag

When the initial filling pressure is 1.5, 2.5, and 3.5 MPa, respectively, and the load is 300 kN, the internal pressure of the fluid bag at different heights is calculated, as shown in Fig.17(a). It can be seen from the figure that the internal pressure of the fluid bag decreases with the increase of height when the initial filling pressure is the same. When the initial filling pressure is different, the change trend of internal pressure is basically the same at different heights, and the change curves are basically parallel.

When the initial filling pressure is 2.5 MPa and the loads are 100, 300, and 500 kN, respectively, the internal pressure of the fluid bag at different heights is calculated, as shown in Fig.17(b); it can be seen from the figure that the internal pressure of the fluid bag decreases with the increase of height



(a) Internal pressure at different initial filling pressures



(b) Internal pressure under different loads

Fig.17 Different initial filling pressure and load on internal pressure at different heights

when the load is the same. When the load is different, the change trend of the internal pressure at different heights is basically the same. When the load is different, the change trend of internal pressure at different heights is basically the same. When the height is small, the difference is large, and when the height is large, the difference is small. Therefore, when the height of the fluid bag is large, the influence of load on internal pressure can be reduced. The increase of the height of the fluid bag will increase the volume of the fluid bag, so the contact area between the liquid bag and the inner and outer shells will also increase. The increase of contact area leads to the increase of the overall stiffness of the mechanism. When the same load is added, the smaller the deformation of the mechanism, the smaller the internal pressure change of the fluid bag.

3.2 Influence of radius on internal pressure of fluid bag

When the initial filling pressure is 1.5, 2.5, and 3.5 MPa, respectively, and the load is 300 kN, the internal pressure of the fluid bag at different radii is calculated, as shown in Fig.18(a). It can be

seen from the figure that when the initial filling pressure is the same, the internal pressure of the fluid bag increases with the increase of the radius. When the initial filling pressure is different, the change trend of internal pressure is basically the same at different radii, and the change curves are basically parallel.

When the initial filling pressure is 2.5 MPa and the loads are 100, 300, and 500 kN, respectively, the internal pressure of the fluid bag at different radii is calculated, as shown in Fig.18(b); it can be seen from the figure that when the load is the same, with the increase of the radius, the internal pressure force of the fluid bag increases. When the load is different, the change trend of internal pressure is basically the same at different radii. The difference of the variation curve is smaller when the radius is small, and the difference is larger when the radius is larger. With the increase of the radius of the fluid bag, the volume of the fluid bag will also increase, which leads to the increase of the overall stiffness of the mechanism. Due to the obvious change of stiffness, there is an obvious difference in the change value of internal pressure.

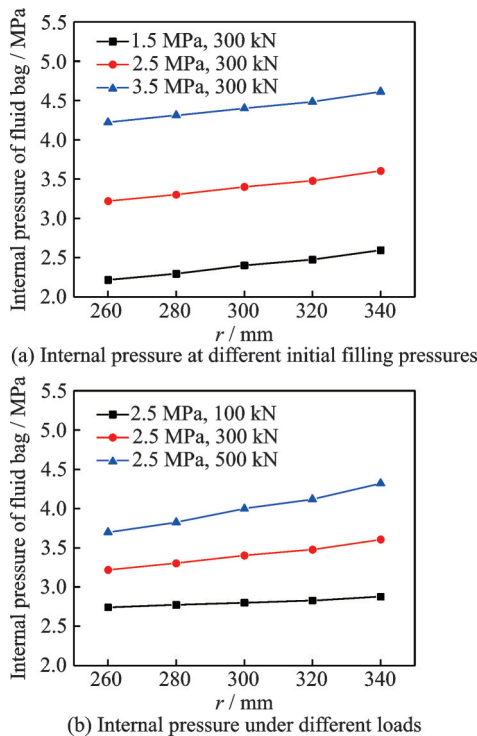


Fig.18 Different initial filling pressure and load on internal pressure at different radii

3.3 Influence of shell thickness on internal pressure of fluid bag

When the initial filling pressure is 1.5, 2.5, and 3.5 MPa, respectively, and the load is 300 kN, the internal pressure of the fluid bag under different shell thicknesses is calculated, as shown in Fig.19(a); it can be seen from the figure that, with the increase of shell thickness, the internal pressure of the fluid bag increases first and then tends to be constant. When the initial filling pressure is different, the change trend of internal pressure is basically the same with different shell thicknesses, and the change curves are basically parallel.

When the initial filling pressure is 2.5 MPa, and the loads are 100, 300, and 500 kN, respectively, the internal pressure of the fluid bag under different shell thicknesses is calculated, as shown in Fig.19(b); it can be seen from the figure that, with the increase of the shell thickness, the internal pressure force of the fluid bag first increases and then tends to be constant. When the load is different, the change trend of internal pressure at different shell thicknesses is basically the same. The difference of variation curves is smaller when the shell thickness

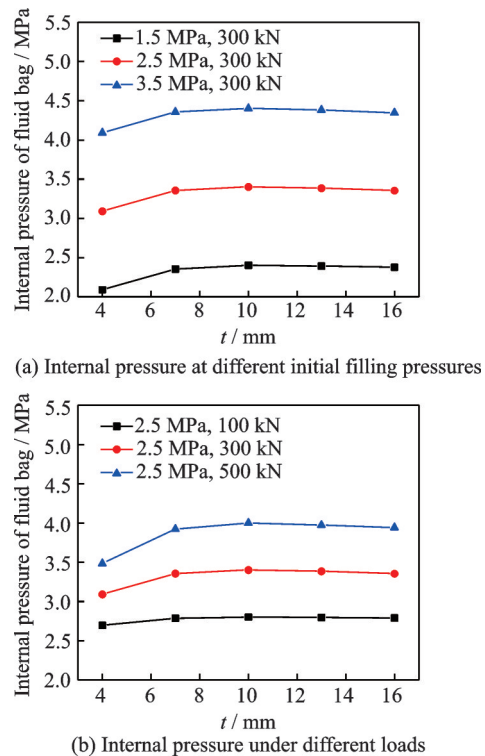


Fig.19 Different initial filling pressure and load on internal pressure at different shell thicknesses

is small, and the difference is larger when the shell thickness is larger. Therefore, when the shell thickness of the fluid bag is small, the influence of load on internal pressure can be reduced.

3.4 Influence of chamfer on internal pressure of fluid bag

When the initial filling pressure is 1.5, 2.5, and 3.5 MPa, respectively, and the load is 300 kN, the internal pressure of the fluid bag under different chamfers is calculated, as shown in Fig.20(a); it can be seen from the figure that the internal pressure of the fluid bag increases slightly with the increase of the chamfer when the initial filling pressure is the same. When the initial filling pressure is different, the change trend of internal pressure in different chamfers is basically the same, and the change curves are basically parallel.

When the initial filling pressure is 2.5 MPa and the loads are 100, 300, and 500 kN, respectively, the internal pressure of the fluid bag under different chamfer conditions is calculated, as shown in Fig.20(b); it can be seen from the figure that when the load is the same, with the increase of the chamfer, the internal pressure of the fluid bag increases slight-

ly. When the load is different, the change trend of internal pressure in different chamfers is basically the same. The difference of variation curves is smaller when the chamfer is small, and the difference is larger when the chamfer is larger. Therefore, when the chamfer of the fluid bag is small, the influence of load on internal pressure can be reduced. However, the chamfer of the fluid bag has little effect on the internal pressure overall, so the proper chamfer can be selected according to the actual situation.

To sum up, it can be seen from Figs.17—20 that the r , t and A are positively proportional to the internal pressure of the fluid bag; and the H is inversely proportional to the internal pressure of the fluid bag.

4 Conclusions

The mechanical characteristics of the new fluid bag buffer mechanism is analyzed and optimized. The sensitivity of the four geometric parameters (r , t , A and H) of the fluid bag is studied by orthogonal experiment method; in order to reduce the displacement of the inner shell, which can enhance the protection effect for the flexible joint, the structure of the buffer mechanism is optimized. Meanwhile, the relevant optimization parameters are obtained. Then, the influence of each parameter on the internal pressure of the fluid bag is analyzed. Finally, the following conclusions can be drawn:

(1) When the fluid bag is impacted, its internal pressure is a rising process of oscillation and fluctuation, and when the impact load reaches the maximum value, its internal pressure reaches the maximum value at the same time.

(2) After optimization, the displacement of the inner shell is reduced by 41.4%, which enhances the protection for the flexible joint; the added value of the internal pressure of the fluid bag is reduced by 13.3%, which enhances the safety of the fluid bag.

(3) According to the results of the orthogonal experiment, the sensitivity of the geometric parameters of the fluid bag to the displacement of the inner shell from high to low is: H , r , t , A .

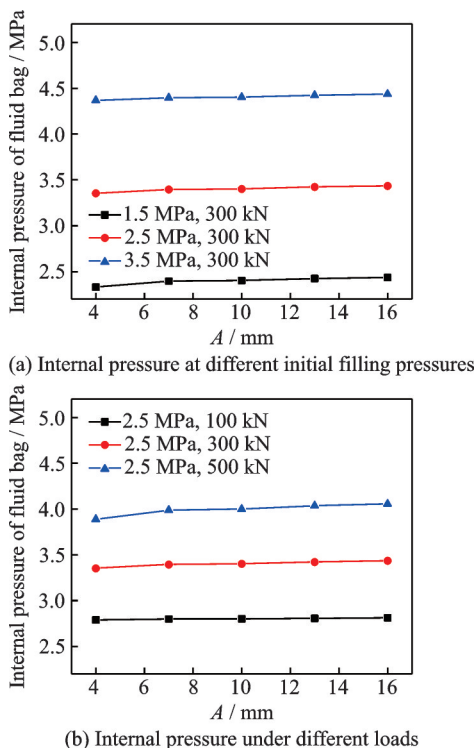


Fig.20 Different initial filling pressure and load on internal pressure at different chamfers

(4) Through the analysis, it can be known that the correlation between the geometric parameters of the fluid bag and its internal pressure is: H has a negative correlation with the internal pressure, while r , t , and A are positively correlated with the internal pressure.

Reference

- [1] TUTT B, SANDY C, CORLISS J. Status of the development of an airbag landing system for the orion crew module: AIAA 2009-2923[R]. [S.l.]: AIAA, 2009: 1-13.
- [2] ERIN C, WILSON B, ZAPFE J. An improve model of a pneumatic vibration isolator: Theory and experiment[J]. Journal of Sound & Vibration, 1998, 218(1): 81-101.
- [3] BERG M. A nonlinear rubber spring model for rail vehicle dynamics analysis[J]. Vehicle System Dynamics, 1998, 30(3/4): 197-212.
- [4] BERG M. A three-dimensional airspring model with friction and orifice damping[J]. Vehicle System Dynamics Supplement, 1999(33): 528-539.
- [5] ODA N, NISHIMURA S. Vibration of air suspension bogie and their design[J]. JSME International Journal, 2008, 13(55): 43-50.
- [6] YUASA T, SAKAI T, HOSOYA H, et al. Application of CAE in the development of air suspension beam[J]. Circulation Journal Official Journal of the Japanese Circulation Society, 1997, 67(1): 93-103.
- [7] LEE H W, HUH H. Finite element analysis of air springs with fiber-reinforced rubber composites using 3-D shell elements[J]. Transactions of the Korean Society of Mechanical Engineers A, 2001, 25(4): 602-609.
- [8] LEE H W, KIM S H, HUH H, et al. Finite element analysis of diaphragm type air springs with fiber-reinforced rubber composites[J]. Journal of Composite Materials, 2003, 37(14): 1261-1274.
- [9] JEONG S H, SONG J H, HUH H, et al. 3-D finite element modeling of fiber reinforced rubber composites using a rebar element[C]//Proceedings of the Fall Conference on Korean Society of Automotive Engineers Spring. [S.l.]: [s.n.], 2007: 1518-1525.
- [10] WONG P K, XIE Zhengchao, ZHAO Jing, et al. Analysis of automotive rolling lobe air spring under alternative factors with finite element model[J]. Journal of Mechanical Science and Technology, 2014, 28(12): 5069-5081.
- [11] OMAN S, NAGODE M. The influence of piston shape on air-spring fatigue life[J]. Fatigue and Fracture of Engineering Materials and Structures, 2017, 41(8): 1019-1031.
- [12] LI Xuebing, WEI Yintao, HE Yuan. Simulation on polytropic process of air springs[J]. Engineering Computations, 2016, 33(7): 1957-1968.
- [13] ZHU Hengjia, YANG Jingzhou, ZHANG Yunqing, et al. A novel air spring dynamic model with pneumatic thermodynamics, effective friction and viscoelastic damping[J]. Journal of Sound & Vibration, 2017(408): 87-104.
- [14] HEINRICH N, DONNER H, IHLEMANN J. Evaluation of air spring textile reinforcement by means of resolving the cord structure in FE analyses[J]. Proceedings in Applied Mathematics and Mechanics, 2017, 17(1): 305-306.
- [15] LI Yan, HE Lin, SHUAI Canggeng, et al. Improved hybrid isolator with maglev actuator integrated in air spring for active-passive isolation of ship machinery vibration[J]. Journal of Sound and Vibration, 2017, 407: 226-239.
- [16] SHIMOZAWA K, TOHTAKE T. An air spring model with non-linear damping for vertical motion[J]. Quarterly Report of Rtri, 2008, 49(4): 209-214.
- [17] XU Liufeng. Mathematical modeling and characteristic analysis of the vertical stiffness for railway vehicle air spring system[J]. Mathematical Problems in Engineering, 2020, 2020(4): 1-12.
- [18] ZHANG Ming, JIANG Rongmin, NIE Hong. Analysis of axial stiffness characteristics of a mechanism of fluid bag shock absorber under alternative factors[J]. Journal of Vibroengineering, 2016, 18(2): 682-698.
- [19] LI Qiji, TENG Liwei, YAN Tianyi, et al. Design of electronic control unit of air spring magneto-rheological suspension system[J]. Journal of Qingdao University (Engineering & Technology Edition), 2019, 34(2): 68-72. (in Chinese)
- [20] ZHANG Ming, JIANG Rongmin, NIE Hong. Analysis of stiffness characteristics of a new fluid bag for axial shock protection[J]. Journal of Vibroengineering, 2015, 17(2): 587-601.

Acknowledgement This work was supported by the Fundamental Scientific Research Business Expenses of Central Universities (No.NJ2020024).

Authors Dr. WANG Hongxian received the M.S. degree in aircraft design and engineering from Nanjing University of Aeronautics and Astronautics, China, in 2010, and he is studying for the Ph.D. degree in aircraft design from Nanjing University of Aeronautics and Astronautics, China, starting

from 2014. His current research interests include aircraft design and landing gear system.

Prof. NIE Hong received the Ph.D. degree in aircraft design from Nanjing University of Aeronautics and Astronautics, Nanjing, China, in 1992. His current research interests include aircraft design, dynamics and landing gear system.

Author contributions Prof. NIE Hong designed the study

and raised the idea. Dr. Wang Hongxian assisted in writing the manuscript. Prof. ZHANG Ming and Dr. HOU Yu contributed to the data for the analysis, and the discussion and background of the study. All authors commented on the manuscript draft and approved the submission.

Competing interests The authors declare no competing interests.

(Production Editor: XU Chengting)

新型流体袋缓冲机构的几何参数对缓冲性能的敏感性分析和优化

王洪宪^{1,2}, 侯 聿³, 张 明², 聂 宏⁴

(1. 南京航空航天大学中小型无人机先进技术工业和信息化部重点实验室, 南京 210016, 中国;

2. 南京航空航天大学飞行器先进设计技术国防重点学科实验室, 南京 210016, 中国;

3. 南京工业职业技术大学航空工程学院, 南京 210023, 中国;

4. 南京航空航天大学机械结构力学及控制国家重点实验室, 南京 210016, 中国)

摘要:设计了一种能在小位移条件下提供轴向大刚度的流体袋缓冲机构。研究了当它受到冲击载荷时,机构的刚度和流体袋内部压力的动态变化规律。针对受冲击过程中对柔性接头的保护性能和流体袋内部的压力变化,采用正交实验设计方法,分析了流体袋各几何参数对轴向刚度影响的敏感性,得出了受冲击时流体袋各几何参数的最优参数组合,该参数组合可以使内壳的位移减少41.4%。结果表明:流体袋受冲击后,其内部压力是一个振荡波动的上升过程;流体袋各几何参数对机构轴向刚度的敏感性高低顺序为:高度 H 、半径 r 、壳厚 t 、倒角 A ;流体袋各几何参数和流体袋内部压力的相关性关系为:高度 H 和内部压力为负相关关系,半径 r 、壳厚 t 、倒角 A 和内部压力为正相关关系。

关键词:缓冲液囊;柔性接头;轴向刚度特性;正交实验法;液囊内压